Publ. Astron. Soc. Japan (2014) 00(0), 1–13
doi: 10.1093/pasj/xxx000

Probing cosmology with weak lensing selected clusters II: Dark energy and $f(R)$ gravity models

Masato SHIRASAKI[1], Takashi HAMANA[1] and Naoki YOSHIDA[2,3,4]

[1]National Astronomical Observatory of Japan, Mitaka, Tokyo 181-8588, Japan
[2]Department of Physics, School of Science, The University of Tokyo, 7-3-1 Hongo, Bunkyo, Tokyo 113-0033, Japan
[3]Kavli Institute for the Physics and Mathematics of the Universe (WPI), Todai Institutes for Advanced Study, The University of Tokyo, Kashiwa, Chiba 277-8583, Japan
[4]CREST, Japan Science and Technology Agency, Kawaguchi, Saitama, Japan

*E-mail: masato.shirasaki@nao.ac.jp

Received ; Accepted

Abstract

Ongoing and future wide-field galaxy surveys can be used to locate a number of clusters of galaxies with cosmic shear measurement alone. We study constraints on cosmological models using statistics of weak lensing selected galaxy clusters. We extend our previous theoretical framework to model the statistical properties of clusters in variants of cosmological models as well as in the standard ΛCDM model. Weak lensing selection of clusters does not rely on the conventional assumption such as the relation between luminosity and mass and/or hydrostatic equilibrium, but a number of observational effects compromise robust identification. We use a large set of realistic mock weak-lensing catalogs as well as analytic models to perform a Fisher analysis and make forecast for constraining two competing cosmological models, wCDM model and $f(R)$ model proposed by Hu & Sawicki, with our lensing statistics. We show that weak lensing selected clusters are excellent probe of cosmology when combined with cosmic shear power spectrum even in presence of galaxy shape noise and masked regions. With the information of weak lensing selected clusters, the precision of cosmological parameter estimate can be improved by a factor of ~ 1.6 and ~ 8 for wCDM model and $f(R)$ model, respectively. Hyper Suprime-Cam survey with sky coverage of 1250 squared degrees can constrain the equation of state of dark energy w_0 with a level of $\Delta w_0 \sim 0.1$. It can also constrain the additional scalar degree of freedom in $f(R)$ model with a level of $|f_{R0}| \sim 5 \times 10^{-6}$, when constraints from cosmic microwave background measurements are incorporated. Future weak lensing surveys with sky coverage of $20,000$ squared degrees will place tighter constraints on w_0 and $|f_{R0}|$ even without cosmic microwave background measurements.

1 INTRODUCTION

Statistical analyses of large astronomical data set have established the standard cosmological model called ΛCDM model. Various statistical methods have been proposed, and have been actually applied to real observational data. Well-known examples include luminosity distance to Type Ia supernovae (Betoule et al. 2014), baryon acoustic oscillation measurement with galaxy clustering (Beutler et al. 2011; Blake et al. 2011; Anderson et al. 2014), the anisotropies of cosmic microwave background (CMB) (Hinshaw et al. 2013; Planck Collaboration et al. 2014), measure of gravitational growth by large-scale structure (Sánchez et al. 2012; Beutler et al.

2014), and weak gravitational lensing (Kilbinger et al. 2013). Although the standard ΛCDM model is consistent with the results from a broad range of cosmological analyses, several alternative models are still allowed at present. In particular, the apparent cosmic acceleration can be explained not only by ΛCDM model but also by a different class of cosmological models that invoke evolving dark energy or modified gravity. Such alternative models are basically constructed by the modification of Einstein equation:

$$G_{\mu\nu} = 8\pi G T_{\mu\nu}. \quad (1)$$

Dark energy models suppose an exotic form of energy in the right hand side of Eq. (1), while modified gravity models changes the left hand side of Eq. (1) without assuming an unknown energy. In order to test the two scenarios, it is essential to measure the gravitational growth of matter density fluctuations, because the modification of gravity could induce characteristic clustering patterns to the matter density distribution in the universe.

Gravitational lensing is one of the most promising tools to probe matter density distribution in the universe. The foreground gravitational field causes small image distortion of distant galaxies. The small distortion contains, collectively, rich cosmological information about the matter distribution. Since image distortion induced by gravitational lensing is very small in general, we require the statistical analysis in order to extract cosmological information from gravitational lensing. Among various statistical methods of gravitational lensing, mapping matter distribution on a continuous sky is a key, basic method (Massey et al. 2007; Van Waerbeke et al. 2013; Chang et al. 2015). The reconstruction is purely based on deflection of light from sources and thus free of conventional astrophysical assumptions. Non-Gaussian features in the reconstructed density field are produced by non-linear gravitational growth and can not be extracted by means of the conventional statistics of cosmic shear such as two-point correlation function or power spectrum.

Clusters of galaxies serve as a promising probe of cosmology. The number count of clusters is expected to be highly sensitive to growth of matter density perturbations (Lilje 1992), whereas correlation analysis of the position of clusters and cosmic shear can constrain both the matter density profile and clustering of clusters (Oguri et al. 2012; Okabe et al. 2013; Covone et al. 2014). The advantage of weak lensing among various techniques is that it does not rely on physical state of the baryonic component in clusters. The finding algorithm with cosmic shear analysis is based on reconstruction of matter density distribution along a line of sight (Hamana, Takada & Yoshida 2004; Hennawi & Spergel 2005; Maturi et al. 2005; Marian et al. 2012). Reconstructed mass density map is utilized to identify high density regions in the universe that correspond to massive collapsed objects such as clusters of galaxies (Miyazaki et al. 2007; Schirmer et al. 2007; Shan et al. 2012).

Previous studies investigated cosmological information in number counts of weak lensing selected clusters (Maturi et al. 2010; Kratochvil, Haiman & May 2010 ; Dietrich & Hartlap 2010; Yang et al. 2011; Hilbert et al. 2012). In our earlier work (Shirasaki et al. 2015, hereafter Paper I), we examined other statistics beyond the abundance of weak lensing selected clusters. There, we study the statistical property of weak lensing selected clusters using realistic mock weak lensing catalogs that incorporate masked regions and shape noise contaminant. We developed a theoretical framework based on halo model that provide robust predictions for the statistical properties of comic shear field and weak lensing selected clusters. In this paper, we derive constrain on variants of cosmological models with the lensing statistics. We extend our theoretical model to predict the lensing statistics for two competing cosmological models (dark energy model and modified gravity model). In order to realize the realistic situation in galaxy imaging surveys, we use two hundreds mock weak lensing catalogs with the proposed sky coverage of ongoing Subaru Hyper Suprime-Cam (HSC) survey[1] (see Paper I for details). We derive accurate covariance matrices between the lensing statistics using our large mock catalogs. We then make realistic forecast for cosmological constraints on two competing scenarios with weak lensing selected clusters.

The paper is organized as follows. In Section 2, we briefly describe the basics of two cosmological models called dark energy model and modified gravity model. There, we describe in detail the evolution of background and linear density perturbations in each model. We also summarize the statistical property of weak lensing selected clusters and the theoretical model of weak lensing statistics in Section 3. By using our theoretical model and a large set of mock catalogs, we make forecast for constraining on cosmological models by our method in the upcoming HSC survey in Section 4. Conclusions and discussions are summarized in Section 5.

2 COSMOLOGICAL MODEL

There exist various extensions to the standard ΛCDM model. We consider two competing models: wCDM model and $f(R)$ model. The former corresponds to a cosmological model based on General Relativity with dark energy and the latter represents a model with modified gravity. Either model can explain the observed acceleration of cosmic expansion at $z \lesssim 1$ with appropriate parameters. Throughout this paper, we assume a spatially flat universe.

[1] http://www.naoj.org/Projects/HSC/index.html

2.1 wCDM model

The expansion of the universe is described by the scale factor $a(t)$. We adopt the usual normalization $a = 1$ at present. In General Relativity under a Friedmann Robertson Walker (FRW) metric, one can derive the time evolution of $a(t)$ as

$$H(a) \equiv \frac{1}{a}\frac{\mathrm{d}a}{\mathrm{d}t} = H_0 \left\{ \Omega_{\mathrm{m0}} a^{-3} + \Omega_{\mathrm{DE}} \times \exp\left[-3 \int_1^a \mathrm{d}a' (1 + w_{\mathrm{DE}}(a'))/a' \right] \right\}^{1/2}, \quad (2)$$

where $H(a)$ is known as the Hubble parameter and $H_0 = 100h\,\mathrm{km\,s^{-1}\,Mpc^{-1}}$ is the present value of $H(a)$. The equation of state of dark energy is specified as $w_{\mathrm{DE}}(a) = P_{\mathrm{DE}}(a)/\rho_{\mathrm{DE}}(a)$ where P_{DE} and ρ_{DE} denote to pressure and density of dark energy, respectively.

In a wCDM model, the linear growth rate of matter density fluctuations after matter domination is given by the solution of the following equation (Wang & Steinhardt 1998):

$$\frac{\mathrm{d}^2 g_+}{\mathrm{d}\ln a^2} + \left[\frac{5}{2} - \frac{3}{2} w_{\mathrm{DE}}(a) \Omega_{\mathrm{DE}}(a) \right] \frac{\mathrm{d}g_+}{\mathrm{d}\ln a} + \frac{3}{2} \left[1 - w_{\mathrm{DE}}(a) \right] \Omega_{\mathrm{DE}}(a) g_+ = 0, \quad (3)$$

where $g_+(a) \equiv D(a)/a$ and $D(a)$ represents the linear growth rate of matter density perturbations. We can obtain $D(a)$ by solving Eq. (3) with the boundary conditions $g_+(a) = 1$ and $\mathrm{d}g_+/\mathrm{d}\ln a = 0$ at $a \ll 1$. The linear density perturbations are commonly characterized by the linear power spectrum $P_{\mathrm{m}}^L(k,a)$. In matter domination, the power spectrum of primordial curvature perturbation is related to that of the matter density through Poisson equation as follows:

$$\frac{4\pi k^3 P_{\mathrm{m}}^L(k,a)}{(2\pi)^3} = \Delta_{\mathcal{R}}^2(k_0) \left(\frac{2c^2k^2}{5H_0^2\Omega_{\mathrm{m0}}} \right)^2 D^2(a) T^2(k) \times \left(\frac{k}{k_0} \right)^{-1+n_s}, \quad (4)$$

$$\Delta_{\mathcal{R}}^2(k) = \frac{4\pi k^3 P_{\mathcal{R}}(k)}{(2\pi)^3}, \quad (5)$$

where $T(k)$ is the transfer function of matter density fluctuations and $P_{\mathcal{R}}(k)$ represents power spectrum of curvature perturbation. In this paper, we normalize P_{m}^L with the value of $A_s \equiv \Delta_{\mathcal{R}}^2(k_0)$ at $k_0 = 0.002\,\mathrm{Mpc}^{-1}$ as follows in Hinshaw et al. (2013).

Throughout this paper, we consider the simplest model of dark energy with constant value of w_0. The non-linear gravitational growth of matter density fluctuations in the model have been investigated by previous numerical studies. For various w_0, a large set of cosmological simulations have been used to derive accurate non-linear power spectrum (Takahashi et al. 2012; Heitmann et al. 2014). Also, Bhattacharya et al. (2011) have studied the abundance of dark matter halos for a wide range of cosmological parameters in wCDM model. In this work, we pay special attention in order to derive observational constraints on w_0 from non-linear cosmological information.

2.2 $f(R)$ model

In $f(R)$ model, the Einstein-Hilbert action is modified by a general function of the scalar curvature R,

$$S_G = \int \mathrm{d}^4x\sqrt{-g} \left[\frac{R + f(R)}{16\pi G} \right]. \quad (6)$$

The action with Eq. (6) leads the modified Einstein equation as

$$G_{\mu\nu} + f_R R_{\mu\nu} - \left(\frac{f}{2} - \Box f_R \right) g_{\mu\nu} - \nabla_\mu \nabla_\nu f_R = 8\pi G T_{\mu\nu}, \quad (7)$$

where $f_R \equiv \mathrm{d}f/\mathrm{d}R$. Assuming a FRW metric, one can determine the time evolution of the Hubble parameter in $f(R)$ model as follows:

$$H^2 - f_R \left(H \frac{\mathrm{d}H}{\mathrm{d}\ln a} + H^2 \right) + \frac{f}{6} + H^2 f_{RR} \frac{\mathrm{d}R}{\mathrm{d}\ln a} = \frac{8\pi G}{3} \rho_m. \quad (8)$$

One can also consider the evolution of matter density perturbations in $f(R)$ model. For sub-horizon modes ($k \gtrsim aH$) in the quasi-static limit[2], the linear growth of matter density perturbations is determined by (Bean et al. 2007)

$$\frac{\mathrm{d}^2 g_+}{\mathrm{d}a^2} + \left(\frac{3}{a} + \frac{1}{H}\frac{\mathrm{d}H}{\mathrm{d}a} \right) \frac{\mathrm{d}g_+}{\mathrm{d}a} - \frac{3\tilde{\Omega}_{\mathrm{m0}} a^{-3}}{(H/H_0)^2 (1 + f_R)} \times \left(\frac{1 - 2Q}{2 - 3Q} \right) \frac{g_+}{a^2} = 0, \quad (9)$$

where $\tilde{\Omega}_{\mathrm{m0}}$ is the effective matter density at present time. We can specify this effective density $\tilde{\Omega}_{\mathrm{m0}}$ as

$$H_{f(R)} = H_0 \left\{ \tilde{\Omega}_{\mathrm{m0}} a^{-3} + \tilde{\Omega}_{\mathrm{DE}} \times \exp\left[-3 \int_1^a \mathrm{d}a' (1 + \tilde{w}_{\mathrm{DE}}(a'))/a' \right] \right\}^{1/2}, \quad (10)$$

where $H_{f(R)}$ is given by Eq. (8). The function Q in Eq. (9) is given by

$$Q(k,a) = -2 \left(\frac{k}{a} \right)^2 \frac{f_{RR}}{1 + f_R}. \quad (11)$$

Note that the function of Q induces non-trivial scale dependence of the linear growth rate $g_+(k,a) = D(k,a)/a$ in $f(R)$ model, while the linear growth rate is solely a function of a in General Relativity.

In this paper, we will consider the representative example of $f(R)$ model proposed by Hu & Sawicki (2007) (hereafter denoted as HS model),

[2] de La Cruz-Dombriz, Dobado & Maroto (2008) have shown that the quasi-static approximation becomes quite reasonable for models with $|f_R| \ll 1$ today.

$$f(R) = -2\Lambda \frac{R^n}{R^n + \mu^{2n}}, \tag{12}$$

where Λ, μ and n are free parameters in the model. For $R \gg \mu^2$, one can approximate the function of $f(R)$ as follows:

$$f(R) = -2\Lambda - \frac{f_{R0}}{n} \frac{\bar{R}_0^{n+1}}{R^n}, \tag{13}$$

where $\bar{R}_0$ is defined by the present scalar curvature of the background space-time and $f_{R0} = -2\Lambda\mu^2/\bar{R}_0^2 = f_R(\bar{R}_0)$. In the HS model with $|f_{R0}| \ll 1$, the background expansion behaves similarly to the standard ΛCDM model. In practice, for $|f_{R0}| \ll 10^{-2}$, geometric tests such as measurement of supernovas cannot distinguish with HS model and the ΛCDM model (Martinelli et al. 2012). Nevertheless, measurement of gravitational growth would be helpful to constrain on HS model if the scale dependence of growth rate as shown in Eq. (9) is detected. The non-linear gravitational growth in HS model have been studied with cosmological simulations (Oyaizu, Lima & Hu 2008; Schmidt et al. 2009a; He, Li & Jing 2013; Zhao 2014). These studies suggest that statistics of galaxy groups or clusters provide meaningful information about the modification of gravity. Therefore, a combination of statistics of cosmic shear and galaxy clusters can offer an interesting probe of HS model. In the following, we focus on the case of $n = 1$ for which many numerical studies have been performed.

3 Weak lensing

Here, we summarize basics of weak gravitational lensing and the finding algorithm of galaxy clusters with weak lensing measurement. Further details of the statistical properties of weak lensing selected clusters are found in Paper I.

3.1 Basics

When considering the observed position of a source object as $\boldsymbol{\theta}$ and the true position as $\boldsymbol{\beta}$, one can express the distortion of image of a source object by the following 2D matrix:

$$A_{ij} = \frac{\partial \beta^i}{\partial \theta^j} \equiv \begin{pmatrix} 1-\kappa-\gamma_1 & -\gamma_2 \\ -\gamma_2 & 1-\kappa+\gamma_1 \end{pmatrix}, \tag{14}$$

where κ is convergence and γ is shear.

Let us consider the case of General Relativity. In this case, one can relate each component of A_{ij} to the second derivative of the gravitational potential as follows (Bartelmann & Schneider 2001; Munshi et al. 2008);

$$A_{ij} = \delta_{ij} - \Phi_{ij}, \tag{15}$$

$$\Phi_{ij} = \frac{2}{c^2} \int_0^\chi \mathrm{d}\chi' g(\chi, \chi') \partial_i \partial_j \Phi(\chi'), \tag{16}$$

$$g(\chi, \chi') = \frac{r(\chi - \chi') r(\chi')}{r(\chi)}, \tag{17}$$

where χ is the comoving distance and $r(\chi)$ represents the comoving angular diameter distance. Gravitational potential Φ can be related to matter density perturbation δ according to Poisson equation. Therefore, convergence can be expressed as the weighted integral of δ along the line of sight;

$$\kappa = \frac{3}{2} \left(\frac{H_0}{c}\right)^2 \Omega_{\mathrm{m}0} \int_0^\chi \mathrm{d}\chi' g(\chi, \chi') \frac{\delta}{a}. \tag{18}$$

Next, we consider weak gravitational lensing effect in HS model. When adopting the Newtonian gauge, one can express the line element as

$$\mathrm{d}s^2 = a(\eta)^2 \left[-(1+2\Phi)\,\mathrm{d}\eta^2 + (1-2\Psi)\,\mathrm{d}\boldsymbol{x}^2 \right], \tag{19}$$

where η is the conformal time. In this metric, the deflection angle by gravitational lensing can be written as (Bartelmann & Schneider 2001; Munshi et al. 2008),

$$\boldsymbol{\alpha} = \frac{2}{c^2} \int \nabla_\perp \left(\frac{\Phi + \Psi}{2} \right) \mathrm{d}\ell, \tag{20}$$

where $\nabla_\perp$ corresponds to the perpendicular component of the gradient along a line of sight for proper distance and $\mathrm{d}\ell$ represents the line integral in terms of proper distance. Considering the modified Einstein equation in HS model with $|\Phi| \ll 1$, $|\Psi| \ll 1$, and $|f_{R0}| \ll 1$, one can derive the following equations of Φ and Ψ (the derivation is found in e.g., Arnold, Puchwein & Springel (2014));

$$\frac{1}{a^2} \nabla^2 \Phi = \frac{16\pi G}{3} \delta\rho - \frac{1}{6} \delta R, \tag{21}$$

$$\frac{1}{a^2} \nabla^2 \Psi = \frac{8\pi G}{3} \delta\rho + \frac{1}{6} \delta R, \tag{22}$$

where ∇ is the gradient with respect to comoving distance and $\delta\rho$ and δR represent the density perturbation and the fluctuation of the scalar curvature R, respectively. Hence, the lensing potential $(\Phi + \Psi)/2$ follows the same equation in General Relativity as

$$\frac{1}{a^2} \nabla^2 \frac{\Phi + \Psi}{2} = 4\pi G \delta\rho. \tag{23}$$

These results show that Eqs. (15), (16) and (18) are available in the HS model with $|f_{R0}| \ll 1$.

3.2 Cluster selection

Weak lensing is a powerful tool to reconstruct the projected matter density field. The conventional technique for reconstruction is based on the smoothed map of cosmic shear. Let us first define the smoothed convergence field as

$$\mathcal{K}(\boldsymbol{\theta}) = \int \mathrm{d}^2\phi\, \kappa(\boldsymbol{\theta} - \boldsymbol{\phi}) U(\boldsymbol{\phi}), \tag{24}$$

where U is the filter function to be specified below. We adopt the compensated Gaussian filter for U as

$$U(\theta) = \frac{1}{\pi\theta_G^2} \exp\left(-\frac{\theta^2}{\theta_G^2}\right) - \frac{1}{\pi\theta_o^2} \left[1 - \exp\left(-\frac{\theta_o^2}{\theta_G^2}\right)\right], \tag{25}$$

where θ_o represents the boundary of the filter and we set U to be zero for $\theta > \theta_o$.

For a given function of U, the power spectrum of a noise convergence field $\mathcal{N}$ is given by (Van Waerbeke 2000)

$$P_{\mathcal{N}}(\ell) = \frac{\sigma_\gamma^2}{2n_{\rm gal}}|\tilde{U}(\ell)|^2 \tag{26}$$

where σ_γ is the rms of the intrinsic source ellipticities $n_{\rm gal}$ represents the number density of source galaxies, and $\tilde{U}$ is the Fourier transform of U. From Eq. (26), we define the moment of $\mathcal{N}$ as

$$\sigma_{{\rm noise},i} = \left(\int \frac{{\rm d}^2\boldsymbol{\ell}}{(2\pi)^2}\ell^{2i}P_{\mathcal{N}}(\ell)\right)^{1/2}. \tag{27}$$

Throughout this paper, we set $\sigma_\gamma = 0.4$, $n_{\rm gal} = 10{\rm arcmin}^{-2}$ and assume the source redshift of $z_{\rm source} = 1$. These are typical values for ground-based galaxy imaging surveys (Heymans et al. 2012). Also, we adopt the smoothing scale of $\theta_G = 5/\sqrt{8\ln 2} = 2.12$ arcmin and $\theta_o = 30$ arcmin. This leads to $\sigma_{{\rm noise},0} \simeq 0.017$. The set up is examined in detail in Paper I with numerical simulations.

On a smoothed lensing map, convergence peaks with high signal-to-noise ratio $\nu = \mathcal{K}/\sigma_{{\rm noise},0}$ are likely caused by galaxy clusters (Hamana, Takada & Yoshida 2004). We thus locate high-ν peaks on a $\mathcal{K}$ map and associate each of them with an isolated massive halo along the line of sight. For a dark matter halo, we assume the universal NFW density profile (Navarro, Frenk & White 1997). We adopt the functional form of the concentration parameter in Duffy et al. (2008),

$$c_{\rm vir}(M,z) = 5.72\left(\frac{M}{10^{14}h^{-1}M_\odot}\right)^{-0.081}(1+z)^{-0.71}. \tag{28}$$

Note that the NFW density profile provides a reasonable fit also for halos in HS model with $|f_{R0}| \ll 1$ (Schmidt et al. 2009a; Lombriser et al. 2012) and that the corresponding convergence κ_h can be calculated analytically (Hamana, Takada & Yoshida 2004).

In order to predict peak heights in a $\mathcal{K}$ map, we adopt the simple assumption that each peak position is exactly at the halo center. Under this assumption, the peak height in absence of shape noise is given by

$$\mathcal{K}_{{\rm peak},h} = \alpha\int {\rm d}^2\phi\, U(\phi;\theta_G,\theta_o)\kappa_h(\phi) + \beta, \tag{29}$$

where $\alpha = 0.9$ and $\beta = 0$ are found to be in good agreement with numerical simulations as shown in Paper I. The actual peak height on a noisy $\mathcal{K}$ map is determined not by Eq. (29), but by a probability distribution function (Fan, Shan & Liu 2010). The probability distribution function of the measured peak height $\mathcal{K}_{\rm peak,obs}$ with a given $\mathcal{K}_{{\rm peak},h}$ is denoted by ${\rm Prob}(\mathcal{K}_{\rm peak,obs}|\mathcal{K}_{{\rm peak},h})$ in this paper. The detailed functional form of ${\rm Prob}(\mathcal{K}_{\rm peak,obs}|\mathcal{K}_{{\rm peak},h})$ is found in Paper I. In Paper I, we show that our model of ${\rm Prob}(\mathcal{K}_{\rm peak,obs}|\mathcal{K}_{{\rm peak},h})$ is quite reasonable for peaks with high signal-to-noise ratio in the case of $\theta_G \sim 2{\rm arcmin}$, $\sigma_\gamma = 0.4$, and $n_{\rm gal} \gtrsim 10{\rm arcmin}^{-2}$.

3.3 Statistics

We here summarize a set of statistics obtained from weak lensing measurement. Table 1 shows the summary of our model of each lensing statistic.

3.3.1 Convergence power spectrum

First, we consider convergence power spectrum, which is a direct probe of the underlying matter density field. Under the Limber approximation[3] (Limber 1954; Kaiser 1992) and Eq. (18), one can calculate the convergence power spectrum as

$$P_{\kappa\kappa}(\ell) = \int_0^{\chi_s}{\rm d}\chi\frac{W_\kappa(\chi)^2}{r(\chi)^2}P_\delta\left(k=\frac{\ell}{r(\chi)},z(\chi)\right), \tag{30}$$

where $P_\delta(k)$ is the three dimensional matter power spectrum, χ_s is comoving distance to source galaxies and $W_\kappa(\chi)$ is the lensing weight function defined as

$$W_\kappa(\chi) = \frac{3}{2}\left(\frac{H_0}{c}\right)^2\Omega_{\rm m0}\frac{r(\chi_s-\chi)r(\chi)}{r(\chi_s)}(1+z(\chi)). \tag{31}$$

The non-linear gravitational growth of $P_\delta(k)$ significantly affects the amplitude of convergence power spectrum at the angular scales less than 1 degree (Jain, Seljak & White 2000; Hilbert et al. 2009; Sato et al. 2009). Therefore, accurate theoretical prediction of the non-linear matter power spectrum is essential for cosmological constraints from weak lensing power spectrum. In order to predict the non-linear evolution of $P_\delta(k)$ for the standard ΛCDM universe, numerical approach based on N-body simulations has been employed extensively over the past few decades (Peacock & Dodds 1996; Smith et al. 2003; Heitmann et al. 2010; Takahashi et al. 2012). In particular, Takahashi et al. (2012) provides an accurate fitting formula of non-linear $P_\delta(k)$ for various wCDM models. We adopt their model in the following. For the HS model of modified gravity, Oyaizu, Lima & Hu (2008); He, Li & Jing (2013); Zhao (2014) investigated the non-linear evolution of $P_\delta(k)$. Recently, Zhao (2014) derived a new fitting formula of non-linear $P_\delta(k)$ with a large set of numerical simulations. We use the model in Zhao (2014) for the HS model.

3.3.2 Convergence peak count

We identify local maxima in a smoothed lensing map and match each peak with a massive dark matter halo along the line of sight. The simple peak count is useful to extract the information of the abundance of massive clusters. One can select the lensing peaks by its peak height. We define the peak signal-to-noise ratio by $\nu = \mathcal{K}_{\rm peak,obs}/\sigma_{{\rm noise},0}$. For a given threshold $\nu_{\rm thre}$, one can predict the surface number density of peaks with $\nu > \nu_{\rm thre}$ as follows (Hamana, Takada & Yoshida 2004):

[3] The validity of Limber approximation have been discussed in e.g., Jeong, Komatsu & Jain (2009). The typical accuracy of Limber approximaion is of a level of $\lesssim$ 1% for $\ell > 10$.

Statistic	Definition	Integrand in halo model	Reference
Convergence power spectrum $P_{\kappa\kappa}$	Eq. (30)	Matter power spectrum P_δ	Takahashi et al. (2012) (wCDM) Zhao (2014) ($f(R)$)
Convergence peak count $N_{\rm peak}$	Eq. (32)	Halo mass function $\mathrm{d}n/\mathrm{d}M$	Bhattacharya et al. (2011) (wCDM) Li & Hu (2011) ($f(R)$)
Convergence peak auto spectrum $P_{\rm pp}$	Eq. (34)	Halo mass function $\mathrm{d}n/\mathrm{d}M$ Linear halo bias b_h	Bhattacharya et al. (2011) (wCDM) Li & Hu (2011) ($f(R)$)
Convergence peak cross spectrum $P_{\rm p\kappa}$	Eqs. (37) and (38)	Halo mass function $\mathrm{d}n/\mathrm{d}M$ Linear halo bias b_h	Bhattacharya et al. (2011) (wCDM) Li & Hu (2011) ($f(R)$)

Table 1. We summarize the elements in our model to derive the lensing statistics presented in this paper. Each column shows, the statistical quantity of interest, the definition, the integrand in our model and the reference of fitting formula to compute the integrand.

$$N_{\rm peak}(\nu_{\rm thre}) = \int \mathrm{d}z\,\mathrm{d}M\,\frac{\mathrm{d}^2V}{\mathrm{d}z\mathrm{d}\Omega}\frac{\mathrm{d}n}{\mathrm{d}M}\,S(z,M|\nu_{\rm thre}), \tag{32}$$

where $\mathrm{d}n/\mathrm{d}M$ represents the mass function of dark matter halo and the volume element is expressed as $\mathrm{d}^2V/\mathrm{d}z\mathrm{d}\Omega = \chi^2/H(z)$ for a spatially flat universe. In Eq. (32), $S(z,M|\nu_{\rm thre})$ expresses the selection function of weak lensing selected clusters for a given threshold of $\nu_{\rm thre}$. It is given by

$$S(z,M|\nu_{\rm thre}) = \int_{\nu_{\rm thre}\sigma_{\rm noise,0}}^{\infty} \mathrm{d}\mathcal{K}_{\rm peak,obs} \times \mathrm{Prob}(\mathcal{K}_{\rm peak,obs}|\mathcal{K}_{{\rm peak},h}(z,M)). \tag{33}$$

Throughout this paper, we adopt the model of halo mass function in Bhattacharya et al. (2011) for wCDM models and the model in Li & Hu (2011) for HS models.

3.3.3 Convergence peak auto spectrum and cross spectrum

Next, we consider the auto-correlation function of peaks and the cross correlation of peaks and convergence. We expect that these statistics contain information of dark matter density profile around clusters as well as of the clustering of clusters.

In Paper I, by using halo model approach, we derive the auto power spectrum of weak lensing selected clusters for a given threshold $\nu_{\rm thre}$ as follows:

$$P_{\rm pp}(\ell) = \int \mathrm{d}\chi\,\frac{W_{\rm p}(\chi|\nu_{\rm thre})^2}{r(\chi)^2}P_m^L\left(k=\frac{\ell}{r(\chi)},z(\chi)\right), \tag{34}$$

where the window function $W_{\rm p}(\chi)$ is given by

$$W_{\rm p}(\chi|\nu_{\rm thre}) = \frac{1}{N_{\rm peak}(\nu_{\rm thre})}\int \mathrm{d}M\,\frac{\mathrm{d}^2V}{\mathrm{d}\chi\mathrm{d}\Omega}\frac{\mathrm{d}n}{\mathrm{d}M} \times S(z,M|\nu_{\rm thre})b_h(z,M), \tag{35}$$

where b_h is the linear halo bias. Similarly, the cross power spectrum between peaks and convergence is given by (also, see Oguri & Takada (2011))

$$P_{\rm p\kappa}(\ell) = P_{\rm p\kappa}^{1h}(\ell) + P_{\rm p\kappa}^{2h}(\ell), \tag{36}$$

$$P_{\rm p\kappa}^{1h}(\ell) = \frac{1}{N_{\rm peak}(\nu_{\rm thre})}\int \mathrm{d}z\,\frac{\mathrm{d}^2V}{\mathrm{d}z\mathrm{d}\Omega} \times \int \mathrm{d}M\,\frac{\mathrm{d}n}{\mathrm{d}M}S(z,M|\nu_{\rm thre})\frac{1}{\bar\rho_m(z)}\frac{W_\kappa(\chi)}{r(\chi)^2} \times M\tilde u_m\left(k=\frac{\ell}{r(\chi)}\middle|z(\chi),M\right), \tag{37}$$

$$P_{\rm p\kappa}^{2h}(\ell) = \int \mathrm{d}\chi\,\frac{W_{\rm p}(\chi|\nu_{\rm thre})W_\kappa(\chi)}{r(\chi)^2} \times P_m^L\left(k=\frac{\ell}{r(\chi)},z(\chi)\right), \tag{38}$$

where $M\tilde u_m$ is the Fourier transform of NFW profile.

In this paper, we adopt the functional form of b_h proposed by Bhattacharya et al. (2011) for wCDM model. For HS models, we derive the linear halo bias based on the peak-background split formalism (Sheth & Tormen 1999). For this purpose, we use the model of mass function shown in Li & Hu (2011) and relate the linear halo bias with mass function as follows:

$$b_h(z,M) = 1 - \frac{\partial \ln f_{\rm MF}}{\partial \delta_c}, \tag{39}$$

where δ_c is the linear critical density for spherical collapse model. $f_{\rm MF}$ is defined by

$$\frac{\mathrm{d}n}{\mathrm{d}M}(z,M) = f_{\rm MF}(z,M)\frac{\bar\rho_m}{M}\left|\frac{\partial \ln \sigma_M^{-1}}{\partial \ln M}\right|, \tag{40}$$

where σ_M is the mass variance for HS models. The functional form of $f_{\rm MF}$ and σ_M are found in Li & Hu (2011).

3.4 Dependence of cosmological model

Figure 1 summarizes the dependence of the weak lensing statistics on cosmological parameters. In order to calculate the lensing statistics for different cosmological models, we use the description summarized in Section 3.3 and Table 1. The four panels in Figure 1 show $P_{\kappa\kappa}$, $P_{\rm pp}$, $P_{\rm p\kappa}$ and $N_{\rm peak}$ for various cosmological models. In each panel, the black line shows the model prediction for ΛCDM model, whereas the colored line represents the model for wCDM models or $f(R)$ models. In this figure, we adopt the value of $w_0 = -0.8$ and -1.2 or $|f_{R0}| = 10^{-4}$ and 10^{-5}. Other cosmological parameters are consistent with those derived by WMAP nine-year analysis (Hinshaw et al. 2013). We also present the ratio of each statistic with respect to the ΛCDM model, i.e., we plot

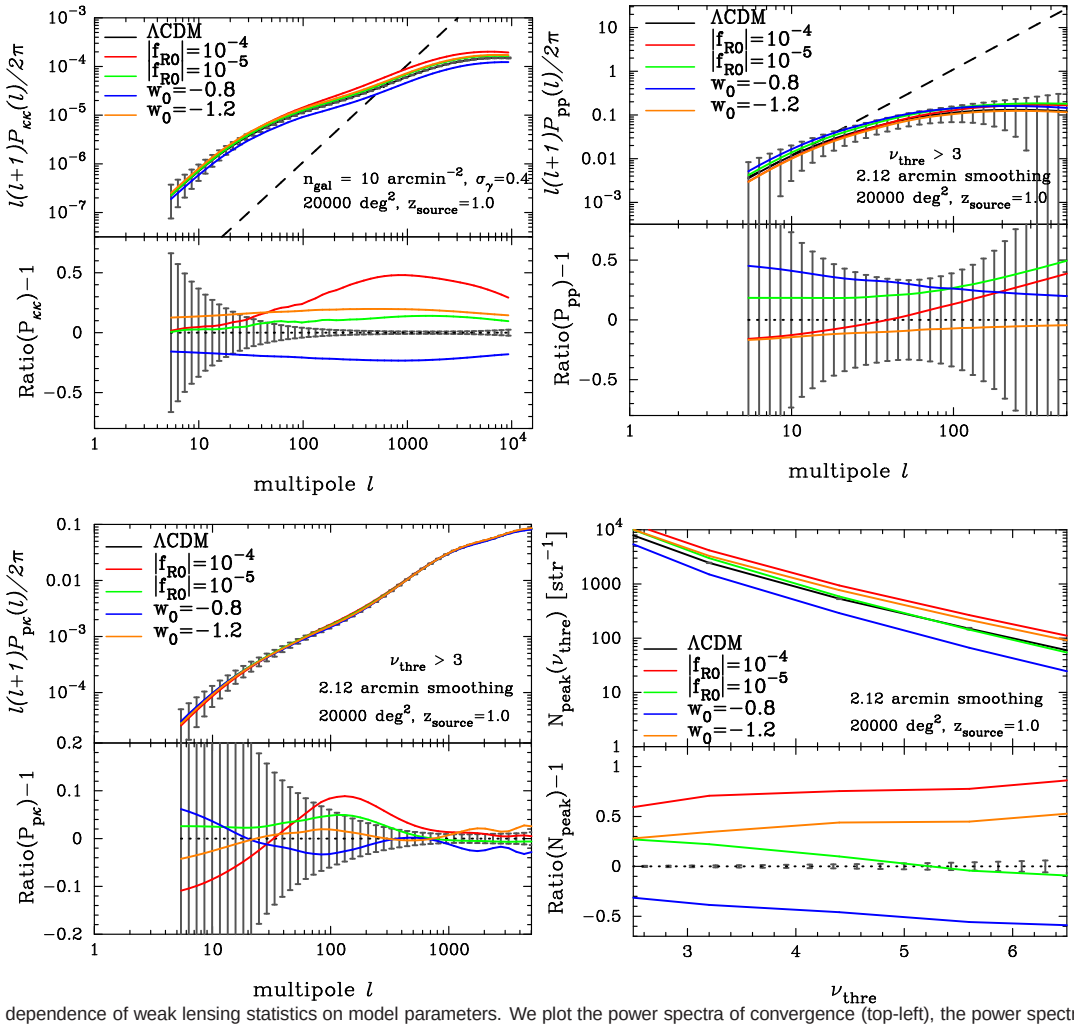

Fig. 1. The dependence of weak lensing statistics on model parameters. We plot the power spectra of convergence (top-left), the power spectra of lensing peaks (top-right), the cross spectra between convergence and lensing peaks (bottom-left), and the number counts of lensing peaks (bottom-left). We define the lensing peaks as those with signal-to-noise ratio $\nu_{\rm thre} > 3$ in the top right and the bottom left panel. The error bars in each panel represent the Gaussian or Poission errors in the case of sky coverage of 20,000 square degrees. The dashed line in two top panels corresponds to the shot noise term of auto power spectrum. In each panel, we show the theoretical model of weak lensing statistics for cosmological models with different value of w_0 and $|f_{R0}|$. The bottom portion in each panel provides the ratio of each statistic between ΛCDM model and wCDM model or $f(R)$ model.

$$\mathrm{Ratio}(X) \equiv \frac{X(w\mathrm{CDM\,or\,HS\,model})}{X_{\Lambda\mathrm{CDM}}}, \tag{41}$$

where $X = P_{\kappa\kappa}, P_{\rm pp}, P_{\rm p\kappa}, N_{\rm peak}$. In Figure 1, we simply consider the Gaussian covariance of power spectra and the Poisson error of the number count of lensing peaks assuming a hypothetical survey with sky coverage of 20,000 squared degrees.

The wCDM model mainly affects the linear growth rate of matter density perturbations and the cosmic expansion rate. Thus, it modifies $P_{\kappa\kappa}$ in an almost scale-independent way and causes larger impact on number of more massive halos, i.e. $N_{\rm peak}$ for higher peaks.

On the other hand, the $f(R)$ model induces the scale-dependence of the linear gravitational growth and reduces gravitational force enhancement as a function of the depth of the gravitational potential wells of dark matter halos. The scale-dependence of growth of linear density fluctuations is determined by the mass of additional scalar degree of freedom f_R in this model. Essentially, the f_R field characterizes two physical length scales: One is the region where the linear growth rate is quite similar to that of ΛCDM and the other is the region where the fluctuation growth is amplified by the additional fifth force. The transition between the two would occur at the compton wavelength of f_R. When density fluctuations grow, another important mechanism, the so-called chameleon mechanism, operates and induces the density dependence of the mass of f_R field. Even at the small length scales where the linear growth rate is amplified, the chameleon mechanism can effectively switch the gravitational force so that ΛCDM-like evolution is recovered. This additional effect would make matter power spectrum and halo mass function more complex. Especially, specific features like bumps are found in the matter power spectrum and in halo mass function on $f(R)$ model (Li & Hu 2011; Zhao 2014).

Therefore, the $f(R)$ model amplifies $P_{\kappa\kappa}$ in a wavenumber dependent manner, and changes appreciably the number of halos with masses near the relevant mass scale of the force enhancement.

Although the error estimate in Figure 1 might seem optimistic, $P_{\kappa\kappa}$ and $N_{\rm peak}$ are expected to be useful to extract cosmological information of the deviation from ΛCDM model. Note, however, that the statistics also depend on parameters other than w_0 and $f_{\rm R0}$. For example, the convergence power spectrum has strong degeneracy among cosmological parameters, while the number of lensing peaks can be much dependent of the concentration of dark matter density profile. In order to overcome the degeneracies and uncertainties, we utilize the cross power spectrum of convergence and lensing peaks $P_{\rm p\kappa}$[4]. The cross correlation can be used to distinguish two different information contents, i.e., cosmological parameters and the dark matter density profile. The former can be mainly extracted from the cross correlation at degree scales whereas the latter can be derived from the cross correlation signals at arcmin scales. Therefore, combined analysis with $P_{\kappa\kappa}, N_{\rm peak}$ and $P_{\rm p\kappa}$ is a powerful tool of cosmology with weak lensing selected clusters.

4 FORECAST

We perform a Fisher analysis to make forecast for constraints on wCDM model or $f(R)$ model with the ongoing Hyper Suprime-Cam (HSC) survey.

Let us briefly summarize the Fisher analysis. For a multivariate Gaussian likelihood, the Fisher matrix F_{ij} can be written as

$$F_{ij} = \frac{1}{2}{\rm Tr}\left[A_i A_j + C^{-1}H_{ij}\right], \tag{42}$$

where $A_i = C^{-1}\partial C/\partial p_i$, $H_{ij} = 2\left(\partial\mu/\partial p_i\right)\left(\partial\mu/\partial p_j\right)$, C is the data covariance matrix, μ represents the assumed model, and $\boldsymbol{p}$ describes parameters of interest. In the present study, we consider only the second term in Eq. (42). Because C is expected to scale proportionally inverse to the survey area, the second term will be dominant for a large area survey (see, e.g., Eifler, Schneider & Hartlap (2009)). We consider the following set of parameters to vary: $\boldsymbol{p} = (10^9 A_s, n_s, \Omega_{\rm m0}, A_{\rm vir,0}, w_0 \,{\rm or}\, |f_{\rm R0}|)$ where $A_{\rm vir,0}$ represents the normalization of concentration of dark matter density profile. We define $A_{\rm vir,0}$ as

$$c_{\rm vir} = A_{\rm vir,0}\left(\frac{M}{10^{14}h^{-1}M_\odot}\right)^{-0.081}(1+z)^{-0.71}. \tag{43}$$

[4] In principle, the auto power spectrum of lensing peaks $P_{\rm pp}$ can be a direct measure of clustering of clusters. However, we find that the signal to noise ratio of $P_{\rm pp}$ is significantly smaller than that of $P_{\rm p\kappa}$. In the case of lensing surveys with the sky coverage of ∼1000 squared degrees, we can find only ~ 100 peaks at most. Thus, the auto-power spectrum $P_{\rm pp}$ would be dominated by the Poisson noise. We expect that $P_{\rm pp}$ can be useful to extract some information only if the survey area exceeds ∼10,000 squared degrees

	$10^9 A_s$	n_s	$\Omega_{\rm m0}$	$A_{\rm vir,0}$	w_0	$10^5\lvert f_{\rm R0}\rvert$
fiducial	2.41	0.972	0.279	5.72	-1	1
$d\boldsymbol{p}$	0.1	0.13	0.01	1.0	0.2	0.5

Table 2. Parameters for Fisher analysis. We denote by $d\boldsymbol{p}$ the variation of parameters around the fiducial vaule that is used for estimation of the numerical derivative of $P_{\kappa\kappa}$, $P_{\rm p\kappa}$ and $N_{\rm peak}$.

We construct the data vector $\boldsymbol{D}$ from a set of binned spectra $P_{\kappa\kappa}, P_{\rm p\kappa}$ and the number count of peaks $N_{\rm peak}$ as,

$$D_i = \{P_{\kappa\kappa}(\ell_1),...,P_{\kappa\kappa}(\ell_{10}), P_{\rm p\kappa}(\ell_1),...,P_{\rm p\kappa}(\ell_{10}), N_{\rm peak}(\nu_{{\rm thre},1}),...,N_{\rm peak}(\nu_{{\rm thre},6})\}, \tag{44}$$

where $P_{\rm p\kappa}$ is defined by the cross spectrum between convergence and lensing peaks with $\nu_{\rm thre} = 3$. For the Fisher analysis, we use 10 bins in the range of $\ell_i = [20, 2000]$ and 6 bins in the range of $\nu_{{\rm thre},i} = [2.5, 5.5]$. In total, a data vector has 26 elements, 2×10 for power- and cross-spectra and 6 for peak counts. In the Fisher analysis, we need the derivative of statistics D_i with respect to $\boldsymbol{p}$. We evaluate the numerical derivatives as follows:

$$\frac{\partial D_i}{\partial p_a} = \frac{D_i(p_a^{(0)} + dp_a) - D_i(p_a^{(0)} - dp_a)}{2dp_a}, \tag{45}$$

where $p_a^{(0)}$ is the fiducial value, dp_a is the variation of a-th parameter and we use the similar definition to $P_{\rm p\kappa}$ and $N_{\rm peak}$. In order to evaluate the term $\partial D_i/\partial p_a$ in Eq. (45), we calculate the relevant statistics adopting the analytic models shown in Section 3.3 and Table 1 for different cosmologies. We summarize the fiducial value of $\boldsymbol{p}$ and $d\boldsymbol{p}$ in Table 2.

We need a 26×26 data covariance matrix for the Fisher analysis. In order to derive the covariances, we use 200 masked sky simulations genearated in Paper I.

The masked sky simulations are constructed based on ten independent full-sky weak lensing simulations. We perform the full-sky weak lensing simulations combined with a large set of dark matter N-body simulations with consistent cosmological model with WMAP nine-year results (Hinshaw et al. 2013). In each simulation, we properly take into account the deflection of light path on a curved sky. From each full-sky realization, we extract multiple "observed" regions with similar survey geometry to the Hyper-Suprime Cam (HSC) survey. We create 20 convergence maps on masked HSC sky by selecting the desired sky coverage (565 + 680 = 1245 squared degrees) from single full-sky simulation. We incorporate the masked regions associated with the positions of bright stars inside the HSC survey regions. The details of the full-sky weak lensing simulations and masked regions are found in Paper I. From 200 realizations of mock HSC data, we construct smoothed convergence maps with the compensated Gaussian filter and fully utilize these maps to derive the covariance matrices between the statistics.

When calculating the inverse covariance, we include a de-

biasing correction as $\alpha = (n_{\rm real} - n_{\rm bin} - 2)/(n_{\rm real} - 1)$ with $n_{\rm rea} = 200$ being the number of realization of simulation sets and $n_{\rm bin} = 26$ being the number of total bins in our data vector (Hartlap, Simon & Schneider 2007).

We also take into account the constraints from the CMB priors expected from the Planck satellite mission. When we compute the Fisher matrix for the CMB, we use the Markov-Chain Monte-Carlo (MCMC) engine for exploring cosmological parameter space `COSMOMC` (Lewis & Bridle 2002). We consider the parameter constraints from the angular power spectra of temperature anisotropies, E-mode polarization and their cross-correlation. For the MCMC analysis, in addition to $10^9 A_s, n_s, \Omega_c h^2$ and w_0, our independent variables include the baryon density $\Omega_b h^2$, Hubble parameter h, reionization optical depth τ, To examine the pure power of weak lensing statistics to constrain w_0 and $|f_{\rm R0}|$, we do not include any constraints on w_0 and $|f_{\rm R0}|$ from the CMB. Assuming that the constraints from the CMB and the lensing statistics are independent, we express the total Fisher matrix as

$$\boldsymbol{F} = \boldsymbol{F}_{\rm lensing} + \boldsymbol{F}_{\rm CMB}. \tag{46}$$

When we include the CMB priors by Eq. (46), we marginalize over the other cosmological parameters except the following three parameters: $10^9 A_s, n_s$, and $\Omega_{\rm m0}$.

Figure 2 summarizes the expected constraints on two cosmological models (wCDM or $f(R)$) in the case of HSC survey. The left panel shows the marginalized 1σ constraints on wCDM models in two-dimensional parameter space and the right panel shows the constraints on $f(R)$ models. In each panel, we indicate constraints (error circles) from different statistics by colored lines.

In the case of wCDM model, there remains strong degeneracy among parameters; especially, it is difficult to break the degeneracy among w_0, A_s and $\Omega_{\rm m0}$ with our statistics alone. This is because we can measure the amplitude of matter density fluctuations by using both $P_{\kappa\kappa}$ and $N_{\rm peak}$ and there apprear no characteristic features in our lensing statistics. In order to break such degeneracies, we require other information such as CMB measurements. When including the information from CMB, we can successfully break the degeneracy among cosmological parameters and thus measure w_0 with a level of $\sim$0.1.

The situation becomes slightly different in the case of $f(R)$ model. The modification of gravitational force due to the additional scalar degree of freedom induces new characteristic features, which can not be compensated by other cosmological parameters. These features are expected to show up as excess of the halo mass function at $M \sim 10^{14}\, h^{-1} M_\odot$ (Li & Hu 2011), or excess in the lensing power spectrum at multipole $\ell \sim 100 - 500$ (Zhao 2014). The relevant mass and length scales of the excess are set by the value of $|f_{R0}|$. Our weak lensing statistics presented here are sensitive and thus one can measure such interesting features using data from upcoming lensing surveys. Interestingly, the expected constraint on $|f_{\rm R0}|$ is at a level of 10^{-5} with our weak lensing statistics *alone*. In addition to our lensing statistics, parameter constraints from CMB measurements would greatly help to break degeneracies among other parameters than $|f_{\rm R0}|$ and $A_{\rm vir,0}$. Since the CMB information provides generally more stringent constraints on n_s and A_s, we can further improve the constraint on $|f_{\rm R0}|$ by combining CMB with our lensing statistics. The expected 1σ error for each parameter is summarized in Table 3.

5 CONCLUSION AND DISCUSSION

We have studied cosmological information content in statistics of weak-lensing selected clusters. We have developed a theoretical model of the lensing statistics and applied to two competing cosmological models: wCDM model and $f(R)$ model. The key parameter in wCDM model and $f(R)$ model are the equation of state parameter of dark energy w_0 and the additional scalar degree of freedom $|f_{\rm R0}|$, respectively. We have utilized masked sky simulations (see Paper I for details) to estimate non-Gaussian covariance caused by non-linear gravitational growth and the mode-coupling due to masked regions simultaneously. With such non-Gaussian covariance, we have performed a Fisher analysis, which yields realistic forecast for constraining the nature of dark energy or the modification of gravity.

We consider specifically ongoing Hyper Suprime-Cam (HSC) survey with a sky coverage of ~ 1250 squared degrees. Combined analysis of cosmic shear and weak lensing selected clusters can constrain w_0 with a level of $\Delta w_0 \sim 0.1$, and $|f_{\rm R0}|$ with a level of $\Delta |f_{\rm R0}| \sim 5 \times 10^{-6}$ with the help of cosmic microwave background measurements. Note that the expected constraint on $|f_{\rm R0}|$ is comparable to the recent constraints of (Cataneo et al. 2014). Clearly, our approach is promising for upcoming surveys with a sky coverage of $10,000$ squared degrees or more. Assuming that the statistical error in upcoming wide field surveys is reduced proportionally to the effective survey area, we can improve the constraints by a factor of $\sim (20000/1250)^{1/2} = 4$ in the case of the Large Synoptic Survey Telescope (LSST)[5] with a proposed sky coverage of 20,000 square degrees. We summarize the expected error with a LSST-like survey in Table 4.

The normalization of power spectrum of matter density perturbations is one of the basic quantities in measure of gravitational growth at low redshift. In practice, we normalize the linear matter power spectrum by using the following quantities:

$$\sigma_R(z) = \left(\int \frac{{\rm d}^3 k}{(2\pi)^3} |W_{\rm TH}(kR)|^2 P_m^L(k,z) \right)^{1/2}, \tag{47}$$

[5] http://www.lsst.org/lsst/

wCDM	$10^9 A_s$	n_s	$\Omega_{\rm m0}$	$A_{\rm vir,0}$	w_0
$P_{\kappa\kappa}$ (HSC)	1.43 (0.0409)	0.111 (0.00385)	0.0918 (0.00192)	– (–)	0.686 (0.0227)
$P_{\kappa\kappa}+P_{\rm p\kappa}$ (HSC)	1.40 (0.0406)	0.109 (0.00381)	0.0897 (0.00190)	1.77 (1.58)	0.676 (0.0225)
$P_{\kappa\kappa}+N_{\rm peak}$ (HSC)	0.548 (0.0338)	0.0830 (0.00331)	0.0728 (0.00170)	1.14 (0.314)	0.469 (0.0193)
$P_{\kappa\kappa}+P_{\rm p\kappa}+N_{\rm peak}$ (HSC)	0.497 (0.0299)	0.0758 (0.00291)	0.0669 (0.00146)	1.02 (0.306)	0.417 (0.0165)
$P_{\kappa\kappa}+P_{\rm p\kappa}+N_{\rm peak}$ (HSC) + Planck	0.132 (0.0294)	0.0145 (0.00274)	0.0124 (0.00143)	0.379 (0.306)	0.108 (0.0165)
$f(R)$	$10^9 A_s$	n_s	$\Omega_{\rm m0}$	$A_{\rm vir,0}$	$10^5\lvert f_{\rm R0}\rvert$
$P_{\kappa\kappa}$ (HSC)	1.35 (0.0386)	0.268 (0.00774)	0.0951 (0.00170)	– (–)	5.91 (0.180)
$P_{\kappa\kappa}+P_{\rm p\kappa}$ (HSC)	1.29 (0.0384)	0.224 (0.00771)	0.0768 (0.00169)	1.82 (1.65)	4.79 (0.178)
$P_{\kappa\kappa}+N_{\rm peak}$ (HSC)	0.571 (0.0309)	0.0168 (0.00372)	0.0311 (0.00146)	1.46 (0.296)	0.897 (0.129)
$P_{\kappa\kappa}+P_{\rm p\kappa}+N_{\rm peak}$ (HSC)	0.418 (0.0267)	0.0136 (0.00297)	0.0219 (0.00133)	0.913 (0.291)	0.717 (0.127)
$P_{\kappa\kappa}+P_{\rm p\kappa}+N_{\rm peak}$ (HSC) + Planck	0.0898 (0.0263)	0.00848 (0.00278)	0.00735 (0.00130)	0.677 (0.291)	0.481 (0.127)

Table 3. The summary of the expected marginalized error with 1σ confidence level. In order to make the forecast of constraints in this table, we assume the following parameters: the rms of intrinsic ellipticies of sources $\sigma_\gamma = 0.4$, number density of sources $n_{\rm gal}=10{\rm arcmin}^{-2}$, and source redshift $z_{\rm source}=1$. For comparison, we also provide the unmarginalized error as the number in brackets.

wCDM	$10^9 A_s$	n_s	$\Omega_{\rm m0}$	$A_{\rm vir,0}$	w_0
$P_{\kappa\kappa}$ (LSST)	0.359 (0.0102)	0.0279 (9.64×10^{-4})	0.0229 (4.80×10^{-4})	– (–)	0.171 (0.00568)
$P_{\kappa\kappa}+P_{\rm p\kappa}$ (LSST)	0.350 (0.0101)	0.0272 (9.53×10^{-4})	0.0224 (4.76×10^{-4})	0.443 (0.395)	0.169 (0.00564)
$P_{\kappa\kappa}+N_{\rm peak}$ (LSST)	0.137 (0.00845)	0.0207 (8.29×10^{-4})	0.0182 (4.26×10^{-4})	0.286 (0.0785)	0.115 (0.00483)
$P_{\kappa\kappa}+P_{\rm p\kappa}+N_{\rm peak}$ (LSST)	0.124 (0.00748)	0.0189 (7.28×10^{-4})	0.0167 (3.67×10^{-4})	0.256 (0.0767)	0.104 (0.00414)
$P_{\kappa\kappa}+P_{\rm p\kappa}+N_{\rm peak}$ (LSST) + Planck	0.0818 (0.00747)	0.0115 (7.25×10^{-4})	0.0101 (3.66×10^{-4})	0.169 (0.0767)	0.0665 (0.00414)
$f(R)$	$10^9 A_s$	n_s	$\Omega_{\rm m0}$	$A_{\rm vir,0}$	$10^5\lvert f_{\rm R0}\rvert$
$P_{\kappa\kappa}$ (LSST)	0.339 (0.00965)	0.0671 (19.3×10^{-4})	0.0237 (4.26×10^{-4})	– (–)	1.47 (0.0452)
$P_{\kappa\kappa}+P_{\rm p\kappa}$ (LSST)	0.322 (0.00960)	0.0562 (19.2×10^{-4})	0.0192 (4.22×10^{-4})	0.455 (0.414)	1.19 (0.0447)
$P_{\kappa\kappa}+N_{\rm peak}$ (LSST)	0.142 (0.00773)	0.00422 (9.30×10^{-4})	0.00779 (3.65×10^{-4})	0.366 (0.0741)	0.224 (0.0324)
$P_{\kappa\kappa}+P_{\rm p\kappa}+N_{\rm peak}$ (LSST)	0.104 (0.00668)	0.00340 (7.41×10^{-4})	0.00586 (3.32×10^{-4})	0.228 (0.0729)	0.179 (0.0319)
$P_{\kappa\kappa}+P_{\rm p\kappa}+N_{\rm peak}$ (LSST) + Planck	0.0655 (0.00667)	0.00285 (7.38×10^{-4})	0.00369 (3.32×10^{-4})	0.204 (0.0729)	0.151 (0.0319)

Table 4. The expected marginalized 1σ error in a LSST-like survey with sky coverage of 20,000 square degrees. We adopt the same parameter as shown in Table 3. We scale the covariance matrices with survey area (i.e. by a factor of $20000/1250$). As for Table 3, the unmarginalized error is shown as the number in brackets.

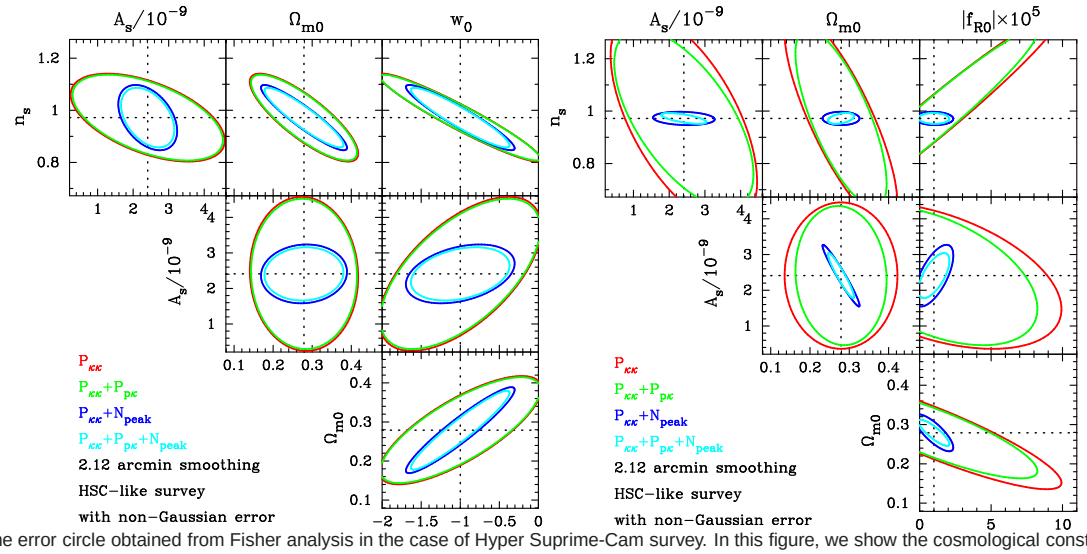

Fig. 2. The error circle obtained from Fisher analysis in the case of Hyper Suprime-Cam survey. In this figure, we show the cosmological constraints from weak lensing statistics alone. Each colored line corresponds to the constraints derived from different statistics: $P_{\kappa\kappa}$ (red), $P_{\kappa\kappa}$ and $P_{\mathrm{p}\kappa}$ (green), $P_{\kappa\kappa}$ and N_{peak} (blue), and combined with three (cyan). The left panel represents the constraint on wCDM model, while the right one shows the constraint on $f(R)$ model. To estimate the constraints presented here, we take into account the non-Gaussian covariances derived from 200 masked sky simulations.

where $W_{TH}(kR)$ is the Fourier transform of top hat function with scale of R and R is commonly set to be 8 $\mathrm{Mpc/h}$. Theoretically, this quantity $\sigma_8(z)$ can be *derived* when the linear matter power amplitude is measured at higher redshift and the linear growth rate is taken into account properly. On the other hand, we can *measure* the value of $\sigma_8(z)$ in a more direct manner when we probe the clustering of matter density field at lower redshift. Therefore, comparing the value of σ_8 derived from high redshift information with the observed σ_8 at lower redshift provides an invaluable opportunity to check consistency of cosmological models between high and low redshift (MacCrann et al. 2014). Figure 3 shows the expected constraint on σ_8 with the lensing statistics proposed in this paper. In this figure, we present the expected constrained region on $\Omega_{\mathrm{m0}} - \sigma_8(z=0)$ plane with 95% confidence level. In order to derive such regions, we sample 100,000 points in five cosmological parameters space for wCDM model (i.e. $A_s, n_s, \Omega_{\mathrm{m0}}, A_{\mathrm{vir},0}$ and w_0) assuming Gaussian distribution function with covariance estimated from Fisher analysis (see, Section 4 for details). Then, we calculate the value of $\sigma_8(z=0)$ at each point. With prior information of CMB measurement, our statistics can constrain on $\sigma_8(z=0)$ with a level of 0.025 and 0.01 for HSC-like and LSST-like survey, respectively. Interestingly, in the case of LSST-like survey, we find that $\sigma_8(z=0)$ can be constrained with precision of $\sim$0.025 even in absence of CMB information. In Figure 3, the square and star symbols represent the derived values of σ_8 for wCDM and $f(R)$ models for a given A_s. For A_s derived from CMB, dark energy and modified gravity model predict the different values of σ_8 from that of the standard ΛCDM model. Thus, the constraint on σ_8 by our lensing statistics serves as an important test on the self-consistency of

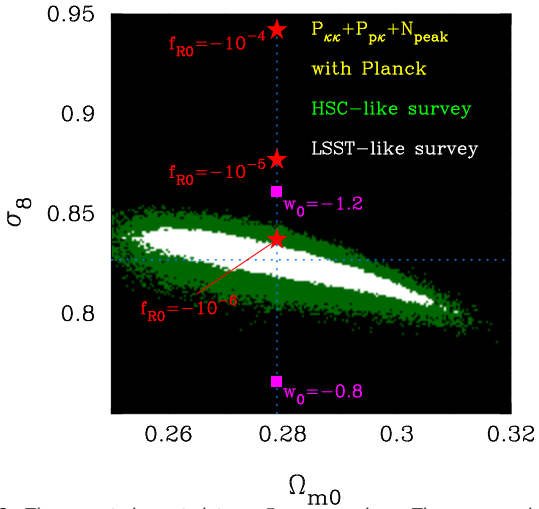

Fig. 3. The expected constraints on $\Omega_{\mathrm{m0}} - \sigma_8$ plane. The green and white region correspond to the marginalized 95% confidence level for HSC and LSST-like survey, respectively. We evaluate these regions from the Fisher matrix in combined analysis of cosmic shear power spectrum, the cross correlation of convergence and its peak, and the number count of peaks with prior information of CMB measurement. The center of confidence surface represent the standard ΛCDM model, while square and star symbols show the different value of σ_8 in wCDM model and $f(R)$ model.

the standard ΛCDM model through $z \sim 1000$ to $z \sim 0$.

Combined statistical analysis with weak lensing selected clusters and cosmic shear provides precise measurement of gravitational growth at low redshift, and thus can place robust constraints on variant cosmological models. However, in order to apply our method to real data set, we need to consider systematic effects in detail. One of the most important systematics is source redshift uncertainty. Throughout this paper, we have

assumed all the source galaxies are located at the same redshift. In reality, source galaxies are distributed over a wide redshift range. In order to examine the effect of source redshift uncertainty, we compare the case of $z_{\rm source} = 0.9$ and $z_{\rm source} = 1$ under ΛCDM cosmology. The 10% difference in the mean source redshift roughly causes under/over-estimate of $\Omega_{\rm m0}$ with a level of ~ 0.01 for cosmic shear power spectrum and cross power spectrum of convergence and its peaks, while the number count of lensing peaks is less sensitive. Therefore, the mean source redshift needs to be calibrated with a level of 0.1 for HSC survey. Clearly, it is important to study the effect of photometric redshift uncertainty in a more quantitative manner, using, for instance, realistic mock galaxy catalogs.

The baryonic processes such as gas cooling and stellar feedback cause bias in parameter estimation with our lensing statistics. Previous studies (Semboloni et al. 2011; Semboloni, Hoekstra & Schaye 2013; Zentner et al. 2013) indicate that the baryonic effect on matter clustering could change two-point statistics of cosmic shear at $\ell \sim 1000$ by a few percent. Since a 3% difference of $P_{\kappa\kappa}$ roughly corresponds to $\Delta\Omega_{\rm m0} \sim 0.015$, the baryonic effect needs to be accounted for in the case of LSST-like survey. For peak statistics, we already take into account a sort of the baryonic effect by considering the uncertainty of halo concentration. We argue that the baryonic processes would cause minor effect on peak statistics for high peaks, as Osato, Shirasaki & Yoshida (2015) have examined. Nevertheless, the detailed modeling of baryonic effect on weak lensing selected clusters will allow to derive more robust constraint on cosmological models.

Massive neutrinos are expected to have a significant effect on cosmic structure formation (e.g., Bond, Efstathiou, & Silk 1980). According to Harnois-Déraps et al. (2015), massive neutrinos with $M_\nu = 0.2$ eV suppress the amplitude of convergence power spectrum at $\ell \sim 1000$ by a factor of ~ 0.9 (see Figure 1 and 2 in Harnois-Déraps et al. (2015)). In addition, Costanzi et al. (2013) have shown massive neutrinos with $M_\nu = 0.2$ eV change the halo mass function with the halo mass of $\sim 10^{14}\, h^{-1} M_\odot$ by a factor of ~ 0.7. Therefore, ignoring massive neutrinos can potentially cause the mis-estimation of σ_8 and/or $\Omega_{\rm m0}$. Further studies on the impact of massive neutrinos on weak lensing statistics are warranted.

Magnification by weak lensing causes the scatter of the brightness and/or the size of source galaxies. This magnification effect on cosmic shear statistics has been investigated in literature (Schmidt et al. 2009b; Schmidt & Rozo 2011; Liu et al. 2014). For convergence power spectrum, Schmidt et al. (2009b) have estimated that the magnification effect typically induces $\sim$1% differences of $P_{\kappa\kappa}$ at $\ell \sim 1000$. On the other hand, the peak height by the NFW dark matter halo is less sensitive to the magnification effect even if one reconstructs the lensing mass map with a smoothing scale of a few arcminutes (e.g., see Figure 5 in Schmidt & Rozo (2011)). The magnification effect on peak statistics would be important in the case of LSST-like survey as Liu et al. (2014) pointed out.

Other than magnification effect, there exist possible systematic effects which could be critical in cosmological analysis with weak lensing selected clusters. Source-lens clustering (Hamana et al. 2002) and the intrinsic alignment (Hirata & Seljak 2004) are likely to compromise cosmological parameter estimation. Although the impact of those effects on cosmic shear statistics is still uncertain, a promising approach in theoretical studies would be associating the source positions with their host dark matter halos on the light cone.

Future galaxy imaging surveys will generate a large amount of high-precision cosmic shear data. It will then become possible to map the matter density distribution in the universe and to measure the growth of the large-scale structure in a direct manner. The lensing statistics studied in this paper will enable us to make the best use of data from future large surveys to explore the origin of cosmic acceleration, or the deviation from the concordance ΛCDM cosmology.

acknowledgments

This work is supported in part by Grant-in-Aid for Scientific Research from the JSPS Promotion of Science (25287050; 26400285). M.S. is supported by Research Fellowships of the Japan Society for the Promotion of Science (JSPS) for Young Scientists. NY acknowledges financial support from JST CREST. Numerical computations presented in this paper were in part carried out on the general-purpose PC farm at Center for Computational Astrophysics, CfCA, of National Astronomical Observatory of Japan.

References

Anderson, L. et al., 2014, MNRAS, 441, 24
Arnold., C., Puchwein., E., Springel., V., 2014, MNRAS, 440, 833
Bartelmann., M., Schneider., P., 2001, Phys. Rep., 340, 291
Bean., R., Bernat., D., Pogosian., L., Silvestri., A., Trodden., M., 2007, Phys. Rev. D, 75, 064020
Betoule., M., et al., 2014, A&A, 568, A22
Beutler., F. et al., 2011, MNRAS, 416, 3017
Beutler., F. et al., 2014, MNRAS, 443, 1065
Bhattacharya., S., Heitmann., K., White., M., Lukić., Z., Wagner., C., Habib., S., 2011, ApJ, 732, 122
Blake., C., et al., 2011, MNRAS, 418, 1707
Bond, J. R. and Efstathiou, G., Silk, J., 1980, Phys. Rev. Lett., 45, 1980
Cataneo., M., et al., 2014, e-print ArXiv:1412.0133
Chang., C., et al., 2015, e-print ArXiv:1505.01871
Costanzi, M., Villaescusa-Navarro, F., Viel, M., Xia, J.-Q., Borgani, S., Castorina, E., Sefusatti, E., 2013, JCAP, 12, 012
Covone., G., Sereno., M., Kilbinger., M., Cardone., V. F., 2014, ApJL, 784, L25

de La Cruz-Dombriz., A., Dobado., A., Maroto., A. L., 2008, Phys. Rev. D, 77, 123515
Dietrich., J. P., Hartlap., J., 2010, MNRAS, 402, 1049
Duffy., A. R., Schaye., J., Kay., S. T., Dalla Vecchia., C., 2008, MNRAS, 390, L64
Eifler., T., Schneider., P., Hartlap., J., 2009, A&A, 502, 721
Fan., Z., Shan., H., Liu., J., 2010, ApJ, 719, 1408
Hamana., T., Colombi., S. T., Thion., A., Devriendt., J. E. G. T., Mellier., Y., Bernardeau., F., 2002, MNRAS, 330, 365
Hamana., T., Takada., M., Yoshida., N., 2004, MNRAS, 350, 893
Hartlap., J., Simon., P., Schneider., P., 2007, A&A, 464, 399
Harnois-Déraps, J., Munshi, D., Valageas, P., van Waerbeke, L., Brax, P., Coles, P., Rizzo, L., 2015, e-print arXiv:1506.06313
He., J.-h., Li., B., Jing., Y. P., 2013, Phys. Rev. D, 88, 103507
Heitmann., K., Lawrence., E., Kwan., J., Habib., S., Higdon., D., 2014, ApJ, 780, 111
Heitmann., K., White., M., Wagner., C., Habib., S., Higdon., D., 2010, ApJ, 715, 104
Hennawi., J. F., Spergel., D. N., 2005, ApJ, 624, 59
Heymans., C., et al., 2012, MNRAS, 427, 146
Hilbert., S., Hartlap., J., White., S. D. M., Schneider., P., 2009, A&A, 499, 31
Hilbert., S., Marian., L., Smith., R. E., Desjacques., V., 2012, MNRAS, 426, 2870
Hinshaw., G., et al., 2013, ApJS, 208, 19
Hirata., C. M., Seljak., U., 2004, Phys. Rev. D, 70, 063526
Hu., W., Sawicki., I., 2007, Phys. Rev. D, 76, 064004
Jain., B., Seljak., U., White., S., 2000, ApJ, 530, 547
Jeong., D., Komatsu., E., Jain., B., 2009, Phys. Rev. D, 80, 123527
Kaiser., N., 1992, ApJ, 388, 272
Kilbinger., M. et al., 2013, MNRAS, 430, 2200
Kratochvil., J. M., Haiman., Z., May., M., 2010, Phys. Rev. D, 81, 043519
Lewis., A., Bridle., S., 2002, Phys. Rev. D, 66, 103511
Li., Y., Hu., W., 2011, Phys. Rev. D, 84, 084033
Lilje., P. B., 1992, ApJL, 386, L33
Limber., D. N., 1954, ApJ, 119, 655
Liu., J., Haiman., Z., Hui., L., Kratochvil., J. M., May., M., 2014, Phys. Rev. D, 89, 023515
Lombriser., L., Koyama., K., Zhao., G.-B., Li., B., 2012, Phys. Rev. D, 85, 124054
MacCrann., N., Zuntz., J., Bridle., S., Jain., B., Becker., M. R., 2014, e-print arXiv:1408.4742
Marian., L., Smith., R. E., Hilbert., S., Schneider., P., 2012, MNRAS, 423, 1711
Martinelli., M., Melchiorri., A., Mena., O., Salvatelli., V., Gironés Z., 2012, Phys. Rev. D, 85, 024006
Massey., R., et al., 2007, Nature, 445, 286
Maturi., M., Angrick., C., Pace., F., Bartelmann., M., 2010, A&A, 519, A23
Maturi., M., Meneghetti., M., Bartelmann., M., Dolag., K., Moscardini., L., 2005, A&A, 442, 851
Miyazaki., S., Hamana., T., Ellis., R. S., Kashikawa., N., Massey., R. J., Taylor., J., Refregier., A., 2007, ApJ, 669, 714
Mohammed., I., Martizzi., D., Teyssier., R., Amara., A., 2014, eprint arXiv:1410.6826
Munshi., D., Valageas., P., Vanwaerbeke., L., Heavens., a., 2008, Phys. Rep., 462, 67
Navarro., J., Frenk., C., White., S., 1997, ApJ, 490, 493
Oguri., M., Bayliss., M. B., Dahle., H., Sharon., K., Gladders., M. D., Natarajan., P., Hennawi., J. F., Koester., B. P., 2012, MNRAS, 420, 3213
Oguri., M., Takada., M., 2011, Phys. Rev. D, 83, 023008
Okabe., N., Smith., G. P., Umetsu., K., Takada., M., Futamase., T., 2013, ApJL, 769, L35
Osato., K., Shirasaki., M., Yoshida., N., 2015, e-print arXiv1501.02055
Oyaizu., H., Lima., M., Hu., W., 2008, Phys. Rev. D, 78, 123524
Peacock., J. A., Dodds., S. J., 1996, MNRAS, 280, L19
Planck Collaboration et al., 2014, A&A, 571, A16
Sánchez., A. G. et al., 2012, MNRAS, 425, 415
Sato., M., Hamana., T., Takahashi., R., Takada., M., Yoshida., N., Matsubara., T., Sugiyama., N., 2009, ApJ, 701, 945
Schirmer., M., Erben., T., Hetterscheidt., M., Schneider., P., 2007, A&A, 462, 875
Schmidt., F., Lima., M., Oyaizu., H., Hu., W., 2009a, Phys. Rev. D, 79, 083518
Schmidt., F., Rozo., E., 2011, ApJ, 735, 119
Schmidt., F., Rozo., E., Dodelson., S., Hui., L., Sheldon., E., 2009b, ApJ, 702, 593
Semboloni., E., Hoekstra., H., Schaye., J., 2013, MNRAS, 434, 148
Semboloni., E., Hoekstra., H., Schaye., J., van Daalen., M. P., McCarthy., I. G., 2011, MNRAS, 417, 2020
Shan., H., et al., 2012, ApJ, 748, 56
Sheth., R., Tormen., G., 1999, MNRAS, 308, 119
Shirasaki., M., Hamana., T., Yoshida., N., 2015, e-print arXiv:1504.05672
Smith., R. E., et al., 2003, MNRAS, 341, 1311
Takahashi., R., Sato., M., Nishimichi., T., Taruya., A., Oguri., M., 2012, ApJ, 761, 152
Van Waerbeke., L., 2000, MNRAS, 313, 524
Van Waerbeke., L., et al., 2013, MNRAS, 433, 3373
Wang., L., Steinhardt., P. J., 1998, ApJ, 508, 483
Yang., X., Kratochvil., J. M., Wang., S., Lim., E. A., Haiman., Z., May., M., 2011, Phys. Rev. D, 84, 043529
Zentner., A. R., Semboloni., E., Dodelson., S., Eifler., T., Krause., E., Hearin., A. P., 2013, Phys. Rev. D, 87, 043509
Zhao., G.-B., 2014, ApJS, 211, 23